LASER INTERFEROMETER GRAVITATIONAL WAVE OBSERVATORY
- LIGO -
CALIFORNIA INSTITUTE OF TECHNOLOGY
MASSACHUSETTS INSTITUTE OF TECHNOLOGY

Technical Note	**LIGO-T2500238-x-0**	2025/09/28

Noise Characterizations in Tabletop Waveguided Optical Parametric Amplification Experiment

Tanisha Ray

California Institute of Technology
LIGO Project, MS 18-34
Pasadena, CA 91125
Phone (626) 395-2129
Fax (626) 304-9834
E-mail: info@ligo.caltech.edu

Massachusetts Institute of Technology
LIGO Project, Room NW22-295
Cambridge, MA 02139
Phone (617) 253-4824
Fax (617) 253-7014
E-mail: info@ligo.mit.edu

LIGO Hanford Observatory
Route 10, Mile Marker 2
Richland, WA 99352
Phone (509) 372-8106
Fax (509) 372-8137
E-mail: info@ligo.caltech.edu

LIGO Livingston Observatory
19100 LIGO Lane
Livingston, LA 70754
Phone (225) 686-3100
Fax (225) 686-7189
E-mail: info@ligo.caltech.edu

http://www.ligo.caltech.edu/

Contents

1 Abstract

Gravitational wave detectors such as Advanced LIGO rely on exquisite sensitivity to detect minuscule spacetime perturbations, making them susceptible to a variety of noise sources. Among the most fundamental is quantum noise, which arises from vacuum fluctuations entering the interferometer's antisymmetric port. To mitigate this limitation, frequency dependent squeezed vacuum states—quantum states with reduced uncertainty in one quadrature—are injected to suppress the quantum noise. Currently, squeezing at LIGO is achieved via optical parametric oscillators (OPOs) using resonant cavities. This project explores Waveguided Optical Parametric Amplification (WOPA) as a cavity-free alternative that offers architectural simplicity and potential robustness against alignment instabilities. WOPA utilizes a single-pass configuration through a periodically poled lithium niobate (PPLN) waveguide, pumped with 532 nm light, to generate broadband squeezed vacuum states at 1064nm.
This work aims to develop a detailed noise and loss budget for the WOPA-based squeezing source. The analysis includes contributions from laser frequency and intensity noise, phase noise, polarization mismatch, propagation and coupling losses in the waveguide, imperfect mode matching, and gain imbalance at the balanced homodyne detector (BHD). The ultimate goal is to identify and limit these noise sources, thereby increasing the achievable level of squeezing.

2 Introduction

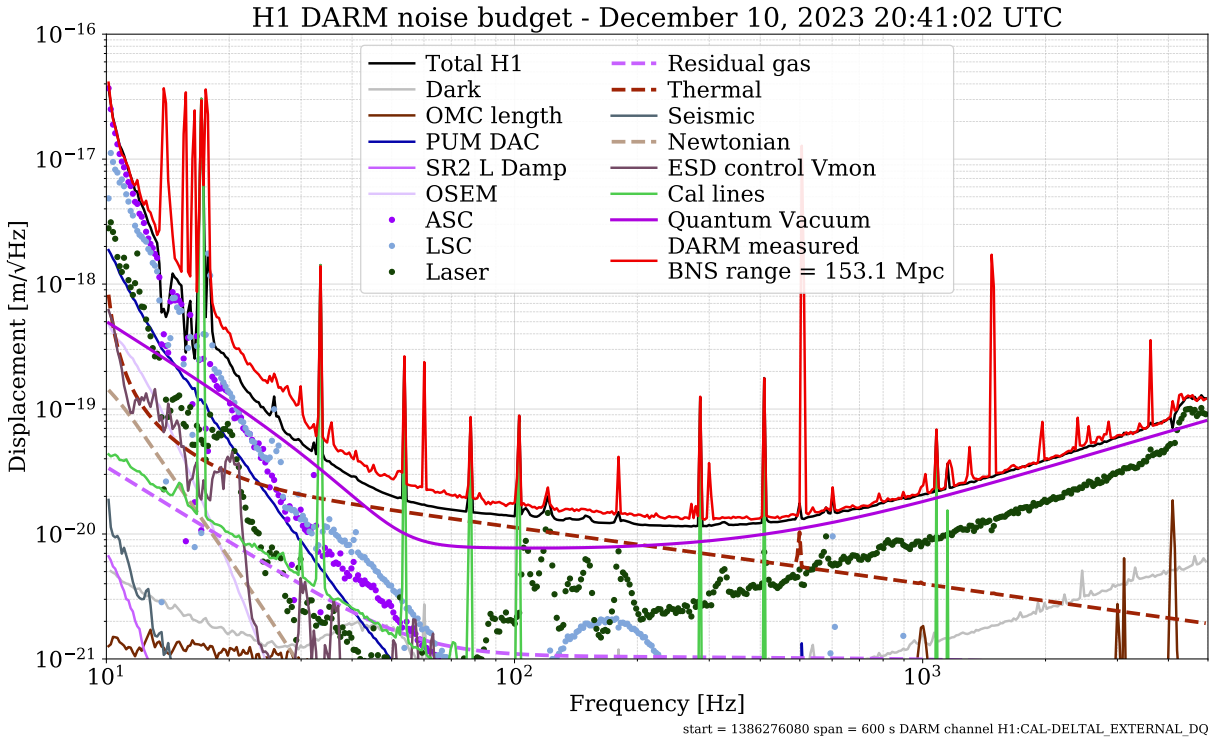

Figure 1: Noise level of the various sources in Advanced LIGO: Hanford Site [8]

Gravitational waves are perturbations or *ripples* in the fabric of space-time, generated by some of the most violent and energetic astrophysical phenomena in the universe. Predicted by Albert Einstein in 1916 as a consequence of his general theory of relativity, gravitational waves arise from the acceleration of massive bodies—such as binary systems of neutron stars or black holes—which distort space-time in a dynamic fashion. These distortions propagate outward at the speed of light, carrying information about their astrophysical origins and providing profound insights into the fundamental nature of gravity.

The Laser Interferometer Gravitational-Wave Observatory (LIGO) is a pioneering facility designed to detect these elusive signals through the technique of laser interferometry. Each LIGO detector comprises two orthogonal arms, each 4 kilometers in length, forming a Michelson interferometer. A laser beam is split at the beam splitter and directed down both arms, where it is reflected off highly isolated mirrors (test masses) before recombination. A passing gravitational wave induces a differential change in arm lengths—stretching one while compressing the other—which leads to a shift in the interference pattern of the recombined light. Measurement of this interference enables the detection and characterization of gravitational wave signals.

LIGO achieves a remarkable strain sensitivity, capable of detecting spacetime distortions as small as $10^{-22}\,\mathrm{m/m}$. This extraordinary sensitivity is fundamentally constrained by **quantum noise**, which limits the detector's performance at both low and high frequencies (Figure 1). Specifically, the quantum fluctuations of the electromagnetic field give rise to amplitude and phase uncertainties at the photodetector readout, which manifest as shot noise at high frequencies and radiation pressure noise at low frequencies.

To mitigate this quantum noise, LIGO employs **squeezed vacuum states**, wherein the electromagnetic ground state is engineered to reduce the uncertainty in either the phase or amplitude quadrature at the expense of the other, consistent with the Heisenberg uncertainty principle. To tailor this squeezing across different frequencies, LIGO utilizes frequency dependent squeezing, made possible through the implementation of 300-meter-long filter cavities that reflect the squeezed vacuum states prior to their injection into the interferometer, allowing the quadrature angle of squeezing to rotate as a function of frequency.

Currently, squeezed vacuum states at LIGO are generated using cavity-based **Optical Parametric Oscillators (OPOs)** [3]. These systems employ nonlinear crystals within optical resonators and have reported producing up to 4 dB (Hanford site) and 5.8 dB (Livingston site) of squeezing. However, these implementations are inherently complex, highly sensitive to optical alignment, and require active stabilization of the cavity length. Such challenges pose limitations in terms of robustness, scalability, and long-term operation of large-scale detectors.

To address these limitations, **Waveguide Optical Parametric Amplification (WOPA)** emerges as a promising alternative that eliminates the need for resonant cavities. By employing a periodically poled lithium niobate (PPLN) waveguide in a single-pass geometry, WOPA significantly simplifies the optical architecture while providing a potentially more stable and compact platform for squeezed light generation.

In this project, we explore the feasibility of WOPA-based squeezing through a tabletop experimental setup. Quantum squeezing at 1064 nm is generated by pumping a PPLN waveguide

with 532 nm light. The resulting squeezed vacuum at 1064 nm is combined with a local oscillator in a Mach-Zehnder-like balanced homodyne detector, enabling direct measurement of the squeezing level. Though WOPA offers an alternative method of generating squeezed states without the need for resonant cavities, the performance of such systems is currently limited by various noise sources and optical losses. Our group's initial implementation has achieved modest squeezing levels of approximately 0.2 dB, which is significantly lower than the ∼4 dB typically achieved in optical parametric oscillator (OPO)-based systems. This discrepancy is largely due to coupling inefficiencies, path length mismatches, mode-matching errors, and the absence of active quantum noise locking.A comprehensive **noise and loss budget** will be developed, accounting for contributions from laser amplitude and phase noise, **coupling and propagation losses in the waveguide**, and inefficiencies in **detection and mode matching**. By rigorously quantifying and minimizing these limiting factors, this work aims to **enhance the observed squeezing level** and assess the viability of WOPA as a replacement for cavity-based systems.

This investigation serves as a critical step toward developing simplified, compact, and robust sources of squeezed light well-suited for future integration into gravitational-wave observatories. Furthermore, the underlying architecture offers promising pathways for broader applications in quantum-enhanced metrology, continuous-variable quantum information processing, quantum neural networks, and coherent feedback control.

3 Overview

In this section, the principal concepts used in this project will be addressed-

3.1 Quantum Noise and Squeezed State Generation

The sensitivity of Advanced LIGO is so great that even the discrete nature of light yields measurable effects. In fact, quantization imposes the most significant barrier to improving LIGO's sensitivity across its entire measurement band. This quantum noise arises fundamentally from the interaction between quantum vacuum fluctuations and the high-power circulating laser field within the interferometer, entering primarily through the readout (dark) port. These vacuum fluctuations are described in terms of the amplitude and phase quadratures of the electromagnetic field, each contributing a distinct form of quantum noise.

Variance in the vacuum's phase quadrature leads to **shot noise**, which is dominant at high frequencies. This noise manifests as fluctuations in photon arrival times at the photodetector, introducing statistical uncertainty in the measurement of small phase shifts caused by passing gravitational waves. At the other end of the spectrum, fluctuations in the amplitude quadrature give rise to **radiation pressure noise**, which becomes significant at low frequencies. This noise manifests as momentum fluctuations of photons reflecting off the suspended test masses, causing perturbations in their positions [2].

These noise mechanisms are fundamentally rooted in the Heisenberg uncertainty principle, reflecting the non-commuting nature of position and momentum observables. Together, they define the Standard Quantum Limit (SQL), which sets the ultimate sensitivity bound

of interferometric measurements in the absence of quantum non-demolition techniques. For a Michelson interferometer, the SQL for strain sensitivity is given by:

$$h_{\mathrm{SQL}} = \sqrt{\frac{4\hbar}{m\Omega^2 L^2}} \tag{1}$$

Here, $\hbar$ is the reduced Planck constant; m denotes the mass of the test mass; Ω is the angular frequency of the signal ($\Omega = 2\pi f$); and L is the length of the interferometer arm.

To surpass this limit, one can employ non-classical states of light known as **squeezed states**, in which quantum noise is redistributed such that uncertainty is reduced in one observable (quadrature) at the expense of the other. The electric field of the optical mode can be decomposed into amplitude (X_1) and phase (X_2) quadratures which relate to the bosonic creation ($a^\dagger$) and anhilation(a) operators via:

$$a = \frac{X_1 + iX_2}{2}, \quad a^\dagger = \frac{X_1 - iX_2}{2} \tag{2}$$

Due to their non-commuting nature, these quadratures obey the uncertainty relation:

$$\Delta X_1 \Delta X_2 \geq 1 \tag{3}$$

In vacuum and coherent states, both quadratures exhibit equal uncertainty ($\Delta X_1 = \Delta X_2 = 1$). Squeezed states, however, achieve reduced uncertainty in one quadrature (< 1) while increasing it in the conjugate quadrature (> 1), thereby preserving the total uncertainty.[4].

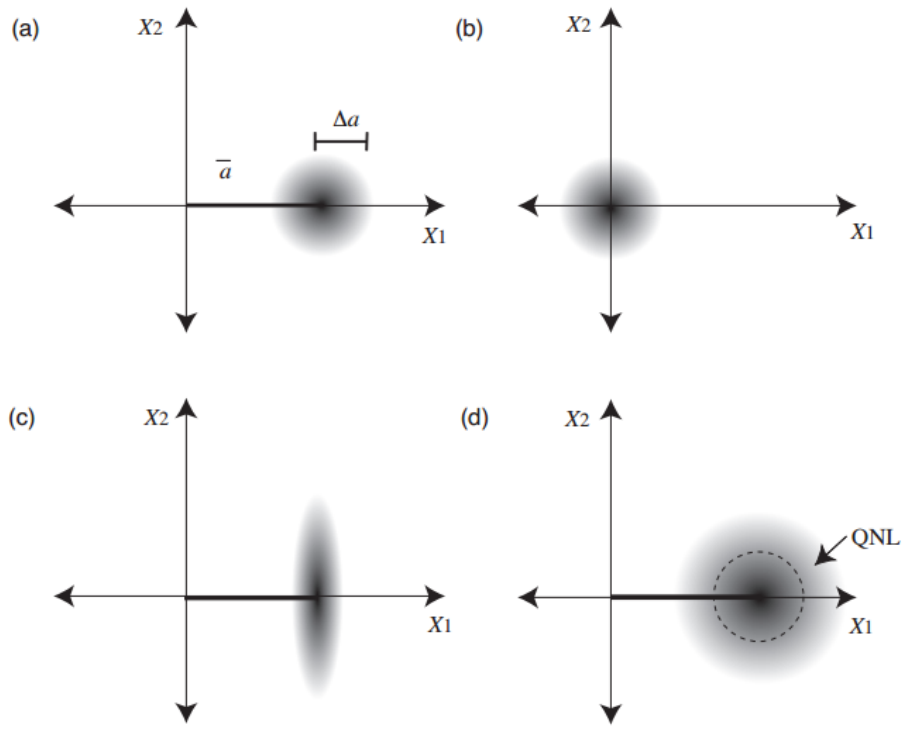

Figure 2: Wigner functions for four states of light: (a) The coherent state, (b) The vacuum state, (c) The amplitude squeezed states, and (d) The classically noisy state[2]

Squeezing is typically generated via nonlinear optical interactions in specialized crystals. When an electric field E is applied to a nonlinear medium, the resulting polarization P of the medium can be expressed as a power series expansion:

$$P = \varepsilon_0 \left(\chi^{(1)} E + \chi^{(2)} E^2 + \chi^{(3)} E^3 + \cdots \right) \tag{4}$$

Here, ε_0 is the vacuum permittivity and $\chi^{(n)}$ is the n^{th}-order nonlinear susceptibility.

he $\chi^{(2)}$ (second-order) nonlinear optical processes include a range of frequency mixing phenomena. Two major classes relevant to this work are:

- **Up-conversion:** $\omega_1 + \omega_2 = \omega_3$
- **Down-conversion:** $\omega_3 = \omega_1 + \omega_2$

When $\omega_1 = \omega_2$ in an up-conversion process, it is called **Second Harmonic Generation (SHG)** and in a down-conversion process, it is called **degenerate Spontaneous Parametric Down-Conversion (SPDC)**. In the process of degenerate SPDC, when an intense and coherent pump field (ω_1) is treated as undepleted and classical, the quantum interaction Hamiltonian takes the form:

$$\hat{H}_{\text{int}} = i\hbar\kappa \left(\hat{a}^{\dagger 2} e^{-i\theta} - \hat{a}^2 e^{i\theta} \right) \tag{5}$$

where κ depends on the nonlinear coefficient and the amplitude of the pump field. This Hamiltonian corresponds to the *single-mode squeezing operator* acting on the vacuum state:

$$|\psi\rangle = \hat{S}(r)|0\rangle \tag{6}$$

with

$$\hat{S}(r) = \exp\left[\frac{1}{2} \left(r e^{-i\theta} \hat{a}^2 - r e^{i\theta} \hat{a}^{\dagger 2} \right) \right] \tag{7}$$

Here, r is the squeezing parameter proportional to the pump intensity and the effective nonlinearity, and θ defines the orientation of the squeezed quadrature in phase space.

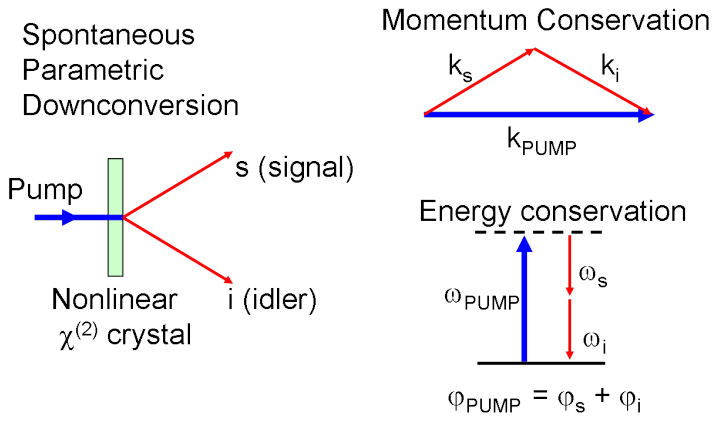

Figure 3: Spontaneous Parametric Down Conversion

Physically, this process arises from the interaction of the intense pump field with the nonlinear medium, which induces a time-varying polarization within the crystal lattice. The $\chi^{(2)}$ nonlinearity couples this oscillating polarization to the quantum vacuum fluctuations present at the signal and idler frequencies. Even in the absence of an input signal, the pump field can spontaneously convert into pairs of indistinguishable photons — signal and idler — conserving both energy and momentum. These photon pairs interfere in a phase-sensitive manner, leading to a redistribution of quantum uncertainty: noise in one quadrature (e.g., amplitude or phase) is reduced below the vacuum level, while the orthogonal quadrature becomes noisier.

Thus, degenerate SPDC produces a **squeezed vacuum state**, which is formally defined as a squeezed state with zero coherent amplitude ($\langle \hat{a} \rangle = 0$).

Optical Parametric Amplification (OPA) is the stimulated counterpart of the SPDC process. In OPA, along with the pump field at frequency ω_p, a coherent signal field (seed) at frequency ω_s is injected into the nonlinear medium. Through the second-order ($\chi^{(2)}$) nonlinearity of the medium, the signal field undergoes phase-sensitive amplification, while an idler field at frequency $\omega_i = \omega_p - \omega_s$ is simultaneously generated to conserve energy. The presence of the seed signal field fundamentally alters the output state: the amplification process is now dependent on the phase relationship between the signal and the pump. OPA produces a **squeezed coherent state** when a seed coherent signal is injected. In the special case where no input signal is injected ($\hat{a}_{\text{in}} = 0$), the OPA process reduces to SPDC and generates a squeezed vacuum state.

In our experiment, we inject a 532 nm beam as pump power into a Periodically Polled Lithium Niobate crystal (PPLN) to create vacuum-squeezed states of 1064 nm via Spontaneous Parametric Down Conversion (SPDC). These vacuum-squeezed states are then detected using balanced homodyne detection.

3.2 Balanced Homodyne Detection

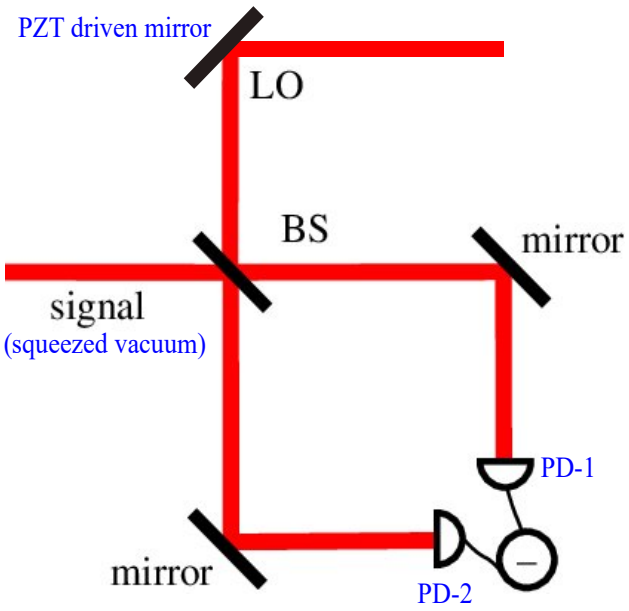

Figure 4: A balanced homodyne detector composed of a 50/50 beamsplitter, a coherent local oscillator (LO) field, and a pair of photodiodes or a balanced photodetector. The input field is a squeezed state of light

The squeezed states generated via SPDC are typically analyzed using Balanced Homodyne Detection (BHD)—the standard method for quadrature measurements of optical fields [3]. The schematic of the setup is given in Figure 4. In BHD, the signal field is combined with a strong reference beam known as the local oscillator (LO) on a symmetric beam splitter. The LO's phase is tuned using a piezoelectric transducer to select the measurement quadrature. The output beams from the splitter are directed to two matched photodiodes (matched via gain balancing), and the resulting photocurrents are electronically subtracted to isolate the quadrature-dependent signal. This differential signal provides direct access to the squeezed quadrature, allowing us to make precise noise measurements in the time domain.

However, the efficacy of BHD is limited by practical imperfections, such as gain imbalance between the photodiodes, path length mismatch between signal and LO arms, and residual technical noises such as laser intensity and phase fluctuations. As such, careful analysis of the BHD readout is essential to accurately quantify the level of squeezing.

3.3 Phase Noise Characterization

In a homodyne detection setup such as the WOPA configuration, the signal beam (carrying squeezed vacuum) and the local oscillator (LO) beam traverse distinct arms of a Mach-Zehnder-type interferometer before recombining at a beamsplitter. When these two arms are not precisely matched in length, the setup becomes susceptible to laser frequency noise, which introduces a time-dependent phase fluctuation into the readout and thereby degrades the observable squeezing.

Let the electric fields of the local oscillator and the squeezed signal be given by:

$$E_{\mathrm{LO}}(t) = E_0\, e^{-i[\omega t + \phi_{\mathrm{LO}}(t)]} \tag{8}$$

$$E_{\mathrm{sig}}(t) = E_0'\, e^{-i[\omega t + \phi_{\mathrm{sig}}(t)]} \tag{9}$$

Let the mismatch in optical path lengths between the LO and signal arms be ΔL. The phase accumulated by each beam over its respective path length depends on the instantaneous optical frequency $\nu(t) = \nu_0 + \delta\nu(t)$, where $\delta\nu(t)$ is the laser frequency noise. The corresponding wavenumber is:

$$k(t) = \frac{2\pi\nu(t)}{c} = \frac{2\pi}{c}(\nu_0 + \delta\nu(t)) \tag{10}$$

Thus, the time-dependent phase acquired along a path of length L is:

$$\phi(t) = k(t)L = \frac{2\pi}{c}\nu(t)L = \underbrace{\frac{2\pi\nu_0 L}{c}}_{\text{static}} + \underbrace{\frac{2\pi\delta\nu(t)L}{c}}_{\text{dynamic}} \tag{11}$$

The phase difference between the two arms is then:

$$\delta\phi(t) = \phi_{\mathrm{LO}}(t) - \phi_{\mathrm{sig}}(t) = \frac{2\pi\nu_0\Delta L}{c} + \frac{2\pi\delta\nu(t)\Delta L}{c} \tag{12}$$

Here, the first term is a static offset, which can be compensated via phase control. The second term is a fluctuating phase shift due to laser frequency noise:

$$\delta\phi(t) \approx \frac{2\pi\Delta L}{c}\delta\nu(t) \tag{13}$$

In our system, the laser exhibits approximately 75 MHz of frequency noise, i.e., $\delta\nu \approx 75 \times 10^6$ Hz. This phase noise rotates the measurement quadrature and mixes the anti-squeezed component into the detected squeezed quadrature, degrading the observed squeezing level.

The measured squeezing level S_{meas} (in dB) in the presence of small phase noise $\delta\phi$ is approximately:

$$S_{\mathrm{meas}} \approx -10\log_{10}\left(e^{-2r}\cos^2\delta\phi + e^{2r}\sin^2\delta\phi\right) \tag{14}$$

where r is the squeezing parameter, and the ideal squeezing level (in dB) is:

$$S_{\mathrm{ideal}} = -10\log_{10}(e^{-2r}) \tag{15}$$

To observe more than 6 dB of squeezing (corresponding to $r \approx 0.69$, $e^{2r} \approx 4$, and $e^{-2r} \approx 0.25$), the phase fluctuation must satisfy $\delta\phi \lesssim 0.14$ rad to limit degradation to under 1 dB. Substituting into the phase noise expression:

$$\Delta L \lesssim \frac{\delta\phi_{\max} \cdot c}{2\pi\,\delta\nu} \tag{16}$$

$$\lesssim \frac{0.14 \cdot 3 \times 10^8\,\mathrm{m/s}}{2\pi \cdot 75 \times 10^6\,\mathrm{Hz}} \tag{17}$$

$$\lesssim 0.089\,\mathrm{m} \approx 8.9\,\mathrm{cm} \tag{18}$$

To observe more than 6 dB of squeezing in the presence of 75 MHz laser frequency noise, the optical path length difference between the LO and signal arms must be maintained below approximately **9 cm**. Minimising this mismatch is essential to suppress phase noise and preserve the integrity of the squeezed state at the readout.

4 Approach

4.1 Experimental Setup

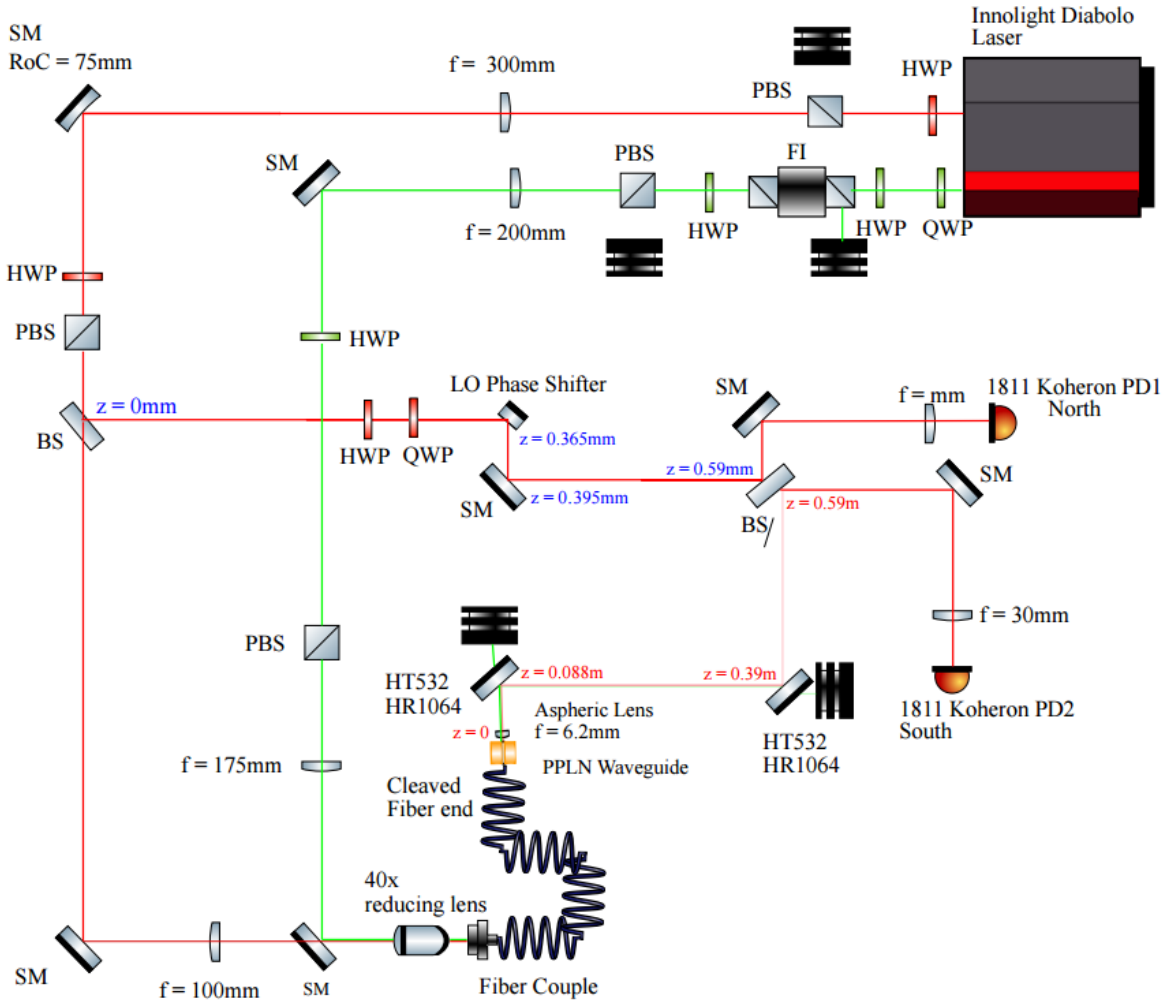

Figure 5: Current WOPA experimental setup

4.1.1 Squeezed State Generation

To generate a squeezed vacuum state, a continuous-wave (CW) single-frequency laser source (Innolight Diabolo) provides both 1064 nm and its frequency-doubled 532 nm output. The 532 nm beam is used for pumping the nonlinear waveguide. To ensure proper polarization and spatial mode quality, the beam is first passed through a half-wave plate (HWP) followed by a polarizing beam splitter (PBS). The HWP is adjusted to rotate the linear polarization axis such that only the desired polarization along the extraordinary axis of the nonlinear crystal is transmitted through the PBS. This is essential for efficient coupling into the nonlinear waveguide, as the nonlinear interaction strength in periodically poled lithium niobate (PPLN) is highly polarization-dependent.

The beam is then guided through a series of optical elements including steering mirrors and lenses. These optics serve to both direct the beam spatially and adjust its beam waist to match the fiber coupling requirements. Another HWP and PBS pair downstream further purifies the polarization and allows for fine-tuning of the pump power by rotating the polarization fraction incident on the PBS. The purified and mode-shaped 532 nm beam is then tightly focused using a 40x microscope objective lens onto the input facet of an optical fiber, which is butt-coupled to the PPLN waveguide.

Within the PPLN waveguide, optical parametric amplification (OPA) occurs: the high-intensity 532 nm pump interacts with vacuum fluctuations to produce a squeezed vacuum state at 1064 nm in the degenerate signal mode via SPDC as described above. The waveguide's tight confinement, quasi-phase-matching, and high nonlinear coefficient make it an excellent platform for generating strong squeezing.

Potential Limitations in Squeezed State Generation:

1. **Polarization Mismatch:** Squeezing is quadrature-selective—amplitude and phase quadratures are orthogonal, and the nonlinear gain is maximized only when the pump polarization aligns with the nonlinear tensor axis of the PPLN. Any misalignment can lead to suboptimal interaction or mixing of quadratures, reducing the observable squeezing. Therefore, it is critical to measure and verify the polarization state of the input pump.
2. **Waveguide Orientation** To verify proper alignment of the fiber and waveguide axis, second harmonic generation (SHG) is used. A polarization-matched(matched using a Waveplate and PBS) 1064 nm beam is sent through the same fiber-waveguide assembly, and the 532 nm SHG output is monitored. Maximizing SHG efficiency provides a practical way to confirm phase-matching and alignment.

4.1.2 Squeezed State Detection

The detection of the squeezed state is performed using a balanced homodyne detection scheme. In this method, the squeezed 1064 nm vacuum field emerging from the PPLN waveguide is combined with a bright 1064 nm local oscillator (LO) on a 50:50 beamsplitter. The LO is derived from the same Diabolo laser by tapping off a fraction of the 1064 nm beam using a polarizing beamsplitter. Its spatial mode and polarization are carefully matched to those of the squeezed field using a combination of half-waveplate, PBS, and lenses.

To enable quadrature selection, a piezo-actuated mirror (LO phase shifter) in the LO path introduces a variable phase shift. This allows the measurement of arbitrary quadratures of the squeezed state by controlling the relative phase between the LO and the signal field.

The two outputs of the beamsplitter are directed to matched low-noise photodiodes (Koheron 1811, labeled PD1 and PD2) via steering mirrors and beam-shaping optics. The outputs of

the photodiodes are electronically subtracted to produce a signal proportional to the quadrature amplitude of the squeezed field.

To measure squeezing in the time domain, the subtracted signal is sent to a lock-in amplifier of Moku. The subtracted signal is split and mixed to obtain sidebands. Then the DC component is extracted using a low pass filter by setting a corner frequency and analyzed. Scanning the LO phase with a sinusoidal drive on the PZT enables reconstruction of the squeezed state and anti-squeezed state levels.

Potential Limitations in Squeezed State Detection:

1. **Mode Mismatch:** Efficient interference between the LO and the squeezed beam requires high spatial mode overlap (visibility). Even minor mismatches in beam waist, divergence, or alignment reduce the interference contrast, effectively mixing in vacuum noise and degrading the measurable squeezing. Therefore, precise mode matching using adjustable lens systems and alignment tools is essential.

2. **Photodiode Gain Imbalance:** Any asymmetry between the gains of the two photodetectors can lead to incomplete subtraction and an artificial increase in the noise floor. This can be corrected through electrical gain balancing or calibration procedures using unsqueezed reference beams.

3. **Phase Drift and PZT Modulation Frequency:** To distinguish true squeezing from slow drifts in the LO-signal relative phase (caused by mechanical or thermal fluctuations), the PZT must be driven at an appropriate frequency. If the modulation is too slow, it becomes difficult to distinguish quantum noise variation from classical phase noise. A carefully selected modulation frequency can ensure reliable quadrature scanning.

4. **Technical Noise Contributions (Moku and PD Noise):** The total noise floor must be below the shot noise to observe squeezing. If the electronic noise from the detection electronics (e.g., Moku system) or the dark noise from photodetectors is comparable to or greater than the shot noise, the squeezing will be masked. Hence, the unsqueezed shot noise level must be calibrated and, if necessary, increased by adjusting the LO power to ensure it dominates over technical noise. Full noise characterization of the detectors and electronics is therefore essential.

Our goal was to generate and characterize squeezed vacuum states using the above-described waveguide-based Optical Parametric Amplification (WOPA) setup and ultimately maximize the squeezing level achieved by optimizing the existing setup. Toward this, it is important to address each of the potential limitations addressed above and overcome them. To do so, we carried out and will be carrying out in the future the following series of experiments to overcome these limitations and achieve decent squeezing levels of the order of 4 dB:

4.2 Polarization Mismatch

Experiment

1) According to the PPLN waveguide datasheet, the fast axis is oriented vertically. To match this, the input beam entering the fiber coupler was vertically polarized using a half-wave plate (HWP) in conjunction with a polarizing beam splitter (PBS). The optical power of this vertically polarized beam was measured using a calibrated power meter.

2) To characterize the polarization state of light entering the crystal, the fiber was deliberately misaligned at the coupling interface with the waveguide. This ensured that light exiting the fiber could be analyzed independently of the waveguide's internal birefringence.

3) A second PBS was introduced after the aspheric lens, at the output side of the waveguide.

4) The power meter was positioned at the reflected (vertically polarized) port of the PBS. The input fiber coupler mount was then rotated while monitoring the power reading. The angle that maximized the reflected power was taken as the orientation corresponding to maximum vertical polarization at the crystal input.

5) The same procedure was repeated for both 1064 nm and 532 nm input beams. The ratio of the power reflected (vertically polarized) to the total transmitted power was taken as a measure of the degree of linear polarization.

Results

- 1064 nm beam: ∼81% linearly polarized in the vertical direction
- 532 nm beam: ∼93% linearly polarized in the vertical direction

Since the field was never at 100% true reflection (vertical polarization) upon rotating the PBS, we infer that the polarization state of the light exiting the fiber is elliptical. Possible causes include:

- Residual mode mixing or imperfect alignment at the fiber-waveguide interface
- Bending-induced mechanical stress in the fiber, leading to birefringence and polarization rotation

Future Follow-up

1) To minimize polarization distortion from the fiber, a new length of polarization-maintaining fiber (P3-1064PM-FC-1) will be cut to multiples of its beat length. The polarization characterization experiment described above will be repeated using this optimized fiber. If significant ellipticity remains, the experimental setup will be modified to reduce fiber bending and mechanical strain.

2) It is also possible that the actual fast axis of the waveguide is not aligned with the nominal vertical direction. Therefore, the polarization angle of the linearly polarized input beam will be systematically varied using a HWP. The polarization orientation that yields the

maximum nonlinear gain—via OPA will be selected for subsequent squeezing experiments. This empirical optimization ensures that the input polarization is correctly aligned with the crystal's effective nonlinear axis.

4.3 Waveguide Orientation

Experiment

To ensure that the fiber coupler and the waveguide are properly aligned for optimal nonlinear interaction, the following measurements were conducted:

1. **Coupling efficiency under unphase matched conditions:** The waveguide was first held at room temperature, a condition under which quasi-phase-matching is not satisfied and no significant nonlinear interaction (e.g., SHG or SPDC) occurs. Under these conditions, the coupling efficiency of the input beam into the PPLN waveguide was determined. This was done by measuring the power of the beam before the 40× focusing lens (input to the bare fiber) and comparing it to the output power measured after the aspheric lens (output from the waveguide). The maximum coupling efficiencies achieved through alignment of the bare fiber with the PPLN input facet were as follows:
   - 1064 nm beam: ∼36% coupling efficiency
   - 532 nm beam: ∼47% coupling efficiency
2. **Phase-matched SHG measurement:**

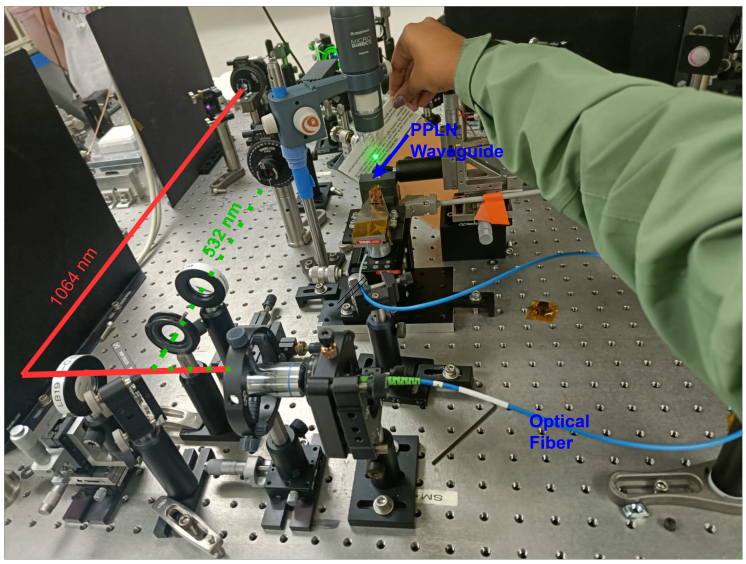

Figure 6: Second harmonic generation in PPLN waveguide

A 1064 nm beam was aligned and coupled into the waveguide. The crystal temperature was then tuned to 52.5°C to achieve quasi-phase-matching for second harmonic generation (SHG). A dichroic mirror was used to separate the generated 532 nm light from

the fundamental. The SHG output power was recorded, and the normalized conversion efficiency was calculated using the following expression:

$$\text{Normalized Conversion Efficiency } \left(\frac{\%}{\text{Watt/cm}^2}\right) = \frac{\dfrac{X_{\text{SHG}}\ [\mu\text{W}]}{(1-R_{\text{OUTPUT}})(1-L_{\text{LOSS}})}}{\left(\dfrac{Y_{\text{PUMP}}\ [\text{mW}]}{(1-R_{\text{OUTPUT}})(1-L_{\text{LOSS}})}\right)^2 \times (L\ [\text{cm}])^2} \times 100\%$$

Here, R_{OUTPUT} (Chip Endface Reflectivity)= 14% [7] and L_{LOSS}(Lens loss)=2%

Result

With an input pump power of 9.5 mW at 1064 nm and a measured SHG output power of 123 μW at 532 nm, the normalized SHG conversion efficiency of the waveguide was found to be approximately 60%/W/cm^2.

Future Follow-up

This method of orienting the waveguide assumes that the polarization and alignment conditions that optimize SHG also correspond to those that maximize spontaneous parametric down-conversion (SPDC), which underlies squeezed light generation. However, this assumption may not hold strictly due to differing phase-matching bandwidths and modal overlaps for SHG and OPA.

To more rigorously optimize the waveguide for squeezing, the nonlinear gain in the SPDC process should be directly maximized. This will be done by launching a high-power 532 nm pump beam along with a low-power 1064 nm seed beam into the waveguide. The amplification of the seed 1064 nm beam through OPA will be measured as a function of pump power and input polarization.

4.4 Mode Matching

Experiment

To achieve efficient balanced homodyne detection (BHD), it is essential that the spatial modes of the local oscillator (LO) and the signal (squeezed vacuum) beam are well overlapped. Mode matching was optimized using a beam profiler to align and match the beam waists and divergence parameters of the LO and signal paths. Through iterative adjustments of lens positions and beam steering mirrors, we achieved beam size agreement within approximately 10–20 μm.

The quality of mode matching was quantified using a time-domain visibility measurement. This involved monitoring the direct current (DC) outputs of each photodiode while phase drifted. The visibility V was calculated using the standard formula:

$$V = \frac{I_{\text{max}} - I_{\text{min}}}{I_{\text{max}} + I_{\text{min}}}$$

Result
The measured BHD visibility was $V \approx 0.6$, indicating a moderately good mode overlap between the LO and the signal beams.

4.5 Photodiode Gain Imbalance

Experiment

To suppress common-mode noise sources—such as residual intensity noise from the laser— it is essential that the outputs of the two photodetectors are accurately gain-matched prior to subtraction. This ensures that only differential quantum fluctuations-shot noise are retained in the signal.

Gain balancing was performed by first blocking the signal path and directing approximately 0.6 mW of 1064 nm LO power onto each photodiode. The subtraction of the AC outputs was implemented digitally using the Moku:Lab's FIR filter builder, with gains adjusted empirically to minimize residual baseline noise. The optimal configuration was:

$$\text{North PD gain: } +1.2 \qquad \text{South PD gain: } -0.9$$

Result

- At low frequencies, some residual peaks remained in the gain-balanced output, likely due to electronic pickup or incomplete subtraction of technical noise.
- At higher frequencies, the output trace was flat, confirming that the detection was shot-noise-limited. This was further validated by comparing the observed noise level to theoretical expectations. The shot noise amplitude spectral density S was estimated using:
$$S = \left(\sqrt{2h\nu P}\right) \cdot (QR)(TRI)(R)(\text{Gain}) \approx 1.33 \times 10^{-6} \, \frac{V}{\sqrt{\text{Hz}}}$$
where h is Planck's constant, ν is the optical frequency, P is the LO power, and the other terms represent detector-specific quantum response, transimpedance gain, reflection coefficients, and amplifier gain. The agreement with theory confirms proper gain balancing and validates the measurement technique.

Therefore, for all future squeezing measurements, the signal will be bandpassed at higher frequencies(MHz range) where the trace is shot-noise-limited. This flat noise floor will be used as the reference against which squeezing below shot noise can be quantified.

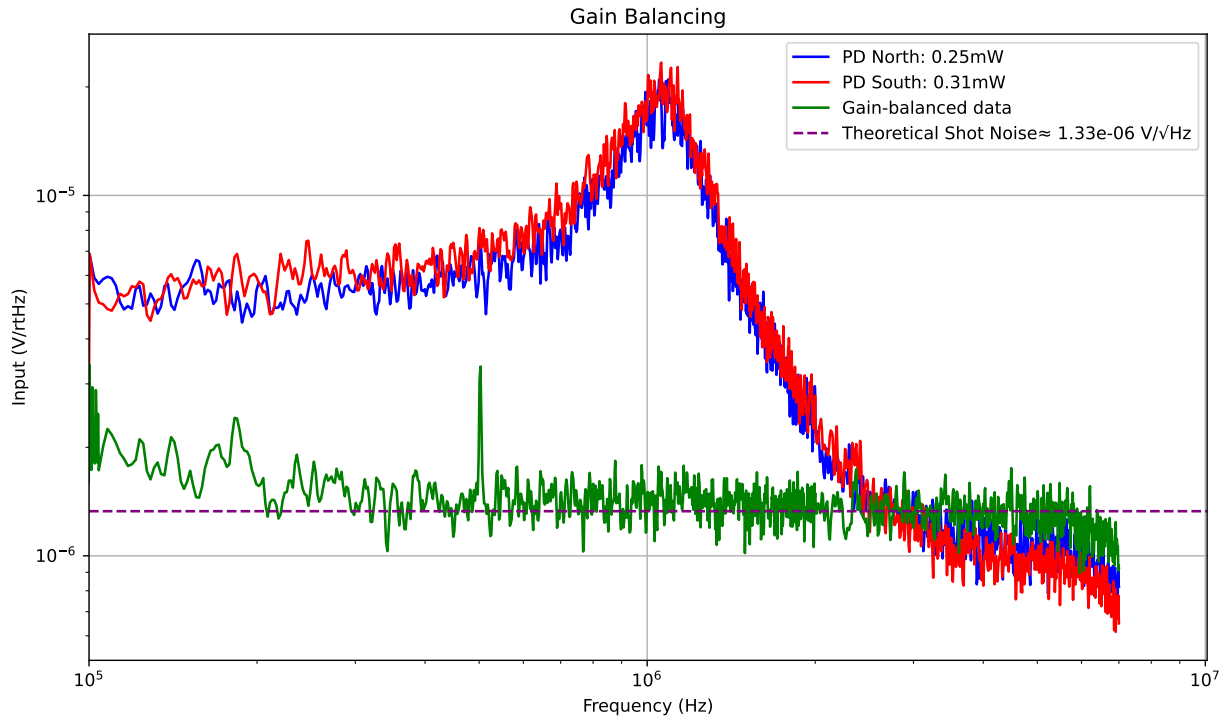

Figure 7: Shot-noise-limited detection after gain balancing. Residual low-frequency peaks are present, while the high-frequency trace is flat and agrees with the theoretical shot noise level.

4.6 Squeezing Measurement

Experiment

After confirming mode matching between the signal and local oscillator (LO) beams, and applying gain balancing to the photodetector outputs as described in the previous sections, we proceeded with the generation and measurement of squeezed vacuum states.

1. **Baseline Shot Noise Calibration:** To establish a reference quadrature variance, we blocked the signal arm and directed only the LO beam onto the two photodiodes. The differential signal, obtained by subtracting the gain-balanced outputs, was then band-passed between 2.5–7 MHz—where the detection is shot-noise limited—and amplified by 5 dB. The filtered and amplified signal was then routed from the Moku:Lab to the Moku:Go via a physical BNC cable.

   In Moku:Go's multi-instrument mode, the Lock-In Amplifier was selected. The input signal was digitally split, assigning both mixer inputs to channel In1, operating in AC mode at 10 Vpp and 0 dB attenuation. Internal modulation was enabled for phase reference. The output of the mixer was low-pass filtered at 500 Hz (18 dB/octave), and the resulting trace was observed on Moku:Go's oscilloscope.

2. **Squeezing Generation:** The 532 nm pump beam was then unblocked, and the maximum available pump power was coupled into the PPLN waveguide. The pump power

measured immediately after the dichroic mirror following the waveguide was approximately 2 mW. The LO power incident on the balanced photodetectors was maintained at 0.6 mW.

3. **Observation of Squeezing:** Upon enabling the 532 nm pump, random phase fluctuations between the squeezed vacuum state and the LO were observed. These manifested as modulations in the quadrature noise signal, seen as fluctuations in the lock-in amplifier's low-pass output. The spontaneous phase drift is attributed to mechanical and thermal fluctuations in the optical paths, causing random sampling of different quadratures of the squeezed state.

   The differential signal (with pump on) was processed in the same way as the shot noise baseline: it was band-passed between 2.5–7 MHz, amplified by 5 dB, and routed to Moku:Go for lock-in detection. The observed baseline quadrature variance was approximately 50 mV under vacuum (unsqueezed) conditions. Upon enabling the pump, modulations around this baseline were observed, corresponding to squeezed and anti-squeezed quadratures.

The levels of squeezing and anti-squeezing, relative to the shot noise baseline, were calculated in decibels using:

$$\text{Level}_{\text{dB}} = 20 \log_{10} \left(\frac{V_{\text{squeezed/anti-squeezed}}}{V_{\text{vacuum}}} \right)$$

Result

Using this relation, we observed:

- Squeezing: ~ -0.14 dB
- Anti-squeezing: $\sim +0.29$ dB

These values confirm the successful generation and detection of squeezed vacuum states.

Following this, the 532 nm pump power was varied systematically, and the corresponding squeezing and anti-squeezing levels were measured. The pump power values reported on the x-axis of the plot were measured immediately after the dichroic mirror following the waveguide. The resulting trend is shown in the following figure:

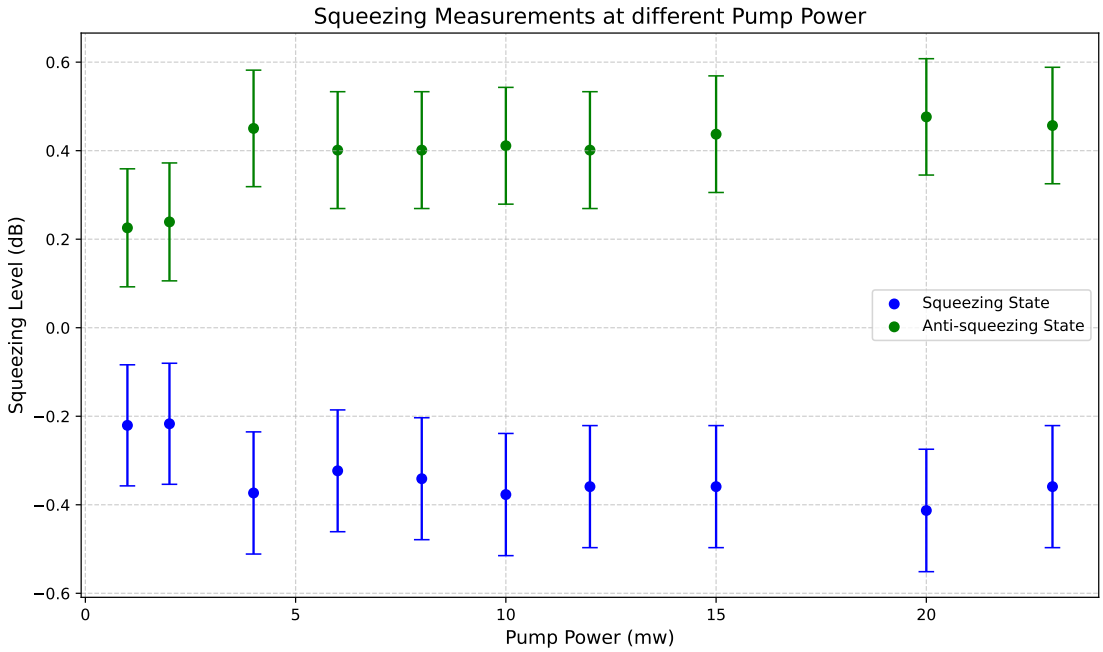

Figure 8: Squeezing level at different pump powers

Squeezing Measurement by Sweeping the PZT in the LO Path

To distinguish true squeezing from slow phase drifts between the signal and local oscillator (LO) beams—caused by mechanical or thermal fluctuations—a piezoelectric transducer (PZT)-mounted mirror was placed in the LO path to enable active phase modulation. This was implemented in three stages:

1. Determining the frequency and voltage requirements for achieving a full-wavelength phase sweep.
2. Characterizing the mechanical response of the PZT by measuring its transfer function and identifying resonant frequencies, after locking out low-frequency phase drifts.
3. Performing squeezing measurements while continuously driving the PZT.

Experiment

Step 1: Characterizing Phase Sweep Range

A 100 Hz triangular waveform (0-10 V) was amplified by a factor of 15(in the PZT driver) and applied to the PZT. The same waveform was also fed into Moku: Go as the reference signal. The resulting phase modulation was confirmed via the interference pattern observed at the balanced homodyne detector (BHD) voltage output in the South PD:

- Slightly more than one wavelength of phase sweep for 75 V input (reference signal was taken by splitting the input, therefore power became half)

- Approximately two wavelengths for 150 V input

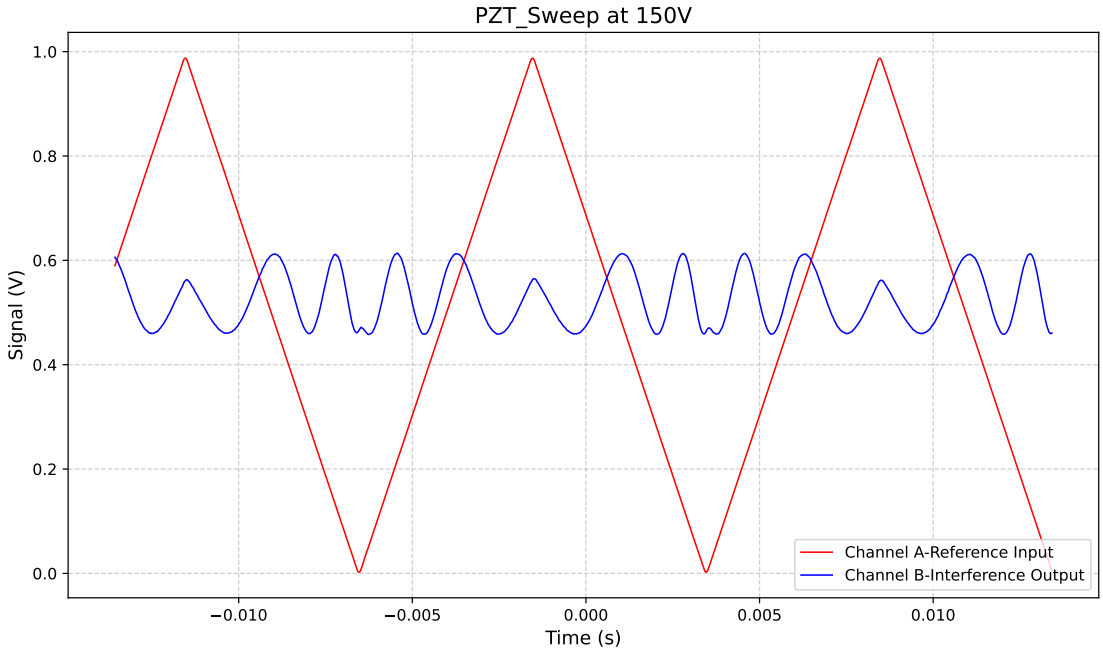

Figure 9: PZT-induced phase sweep at 150 V input

This range enables observation of two full squeezing and anti-squeezing cycles within a single triangular sweep, allowing time-domain tomography of the squeezed quadrature.

Step 2: Locking Drift Noise to measure the transfer function

To characterize the PZT-mounted mirror's transfer function and avoid mechanical resonances during operation, we first designed a feedback loop that can suppress low-frequency drift noise and actuate the PZT with an external signal. The block diagram of the feedback loop is shown below:

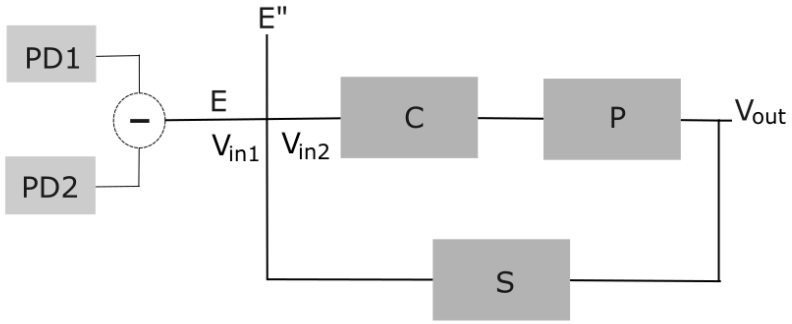

Figure 10: Feedback loop for drift noise suppression

Here,

- E: Error signal (Output from PD1 - PD2).
- C: Controller (Integrator in Moku PID).
- P: Plant (PZT including mechanical mirror response).
- E": Excitation (Sin Wave).
- S: Sensor.

Initially, only the drift noise locking part was implemented as follows-

- The error signal (DC difference between North and South photodiodes) was fed into a Controller (integrator in Moku-Pro's PID module).
- The controller output was amplified using an SRS-560 preamplifier and the PZT driver with gains of 10 V/V and 15 V/V respectively.

Attempts to lock the drift noise using Moku alone were unsuccessful due to insufficient output voltage. However, incorporating the SRS-560 amplifier enabled stable locking, as evidenced by the clean transition from unlocked to locked state on turning on the controller signal.

Step 3: Determining the Transfer Function Using Frequency Response Analysis

To characterize the frequency response of the PZT-mounted mirror and identify any mechanical resonances, we employed frequency-domain analysis under a drift-locked condition.

Assumptions:

- $C(f)$: Transfer function of the controller (integrator)
- $P(f)$: Transfer function of the plant (PZT + mirror)
- $S(f)$: Sensor transfer function (assumed unity: $S(f) = 1$)
- V_{in1}: Error signal after applying excitation
- V_{in2}: Combined input to the plant (error + excitation)

The open-loop transfer function of the system can be expressed as-

$$G_{\text{open}}(f) = \frac{V_{\text{in1}}}{V_{\text{in2}}} = C(f) \cdot P(f) \cdot S(f)$$

$$\Rightarrow \log P(f) = \log\left(\frac{V_{\text{in1}}}{V_{\text{in2}}}\right) - \log C(f)$$

Thus, by measuring V_{in1} and V_{in2} and subtracting the known contribution of the controller $C(f)$, we can isolate and compute the plant's frequency response $P(f)$.

To implement this, the Moku-Pro's multi-instrument interface was configured with three PID controllers and a Frequency Response Analyzer (FRA). The setup enabled us to inject known sine wave excitations into the locked feedback loop and compute the plant's response over a range of frequencies via the above relation.

Configuration in the Moku-Pro's multi-instrument interface was as follows:

- **PID 1:** Inputs 1 and 2 received DC outputs from the North and South PDs. These were subtracted to produce an error signal V_{in1}.
- **PID 2:** Input 1 was V_{in1}. Input 2 was an excitation sine wave from the FRA. The sum, V_{in2}, was fed to PID 3.
- **PID 3:** V_{in2} was integrated to act as the controller. The gain-frequency (i.e., the integrator's zero gain-cross frequency) was tuned to 1 kHz and 1.175 kHz in different trials.
- **FRA:** Inputs 1 and 2 received V_{in1} and V_{in2}, respectively. The output was a frequency-swept sine wave fed to PID 2. The FRA computed the transfer function magnitude as

$$\log|G(f)| = \log\left(\frac{V_{\text{in1}}}{V_{\text{in2}}}\right),$$

representing the combined frequency response of the controller and plant (PZT system).

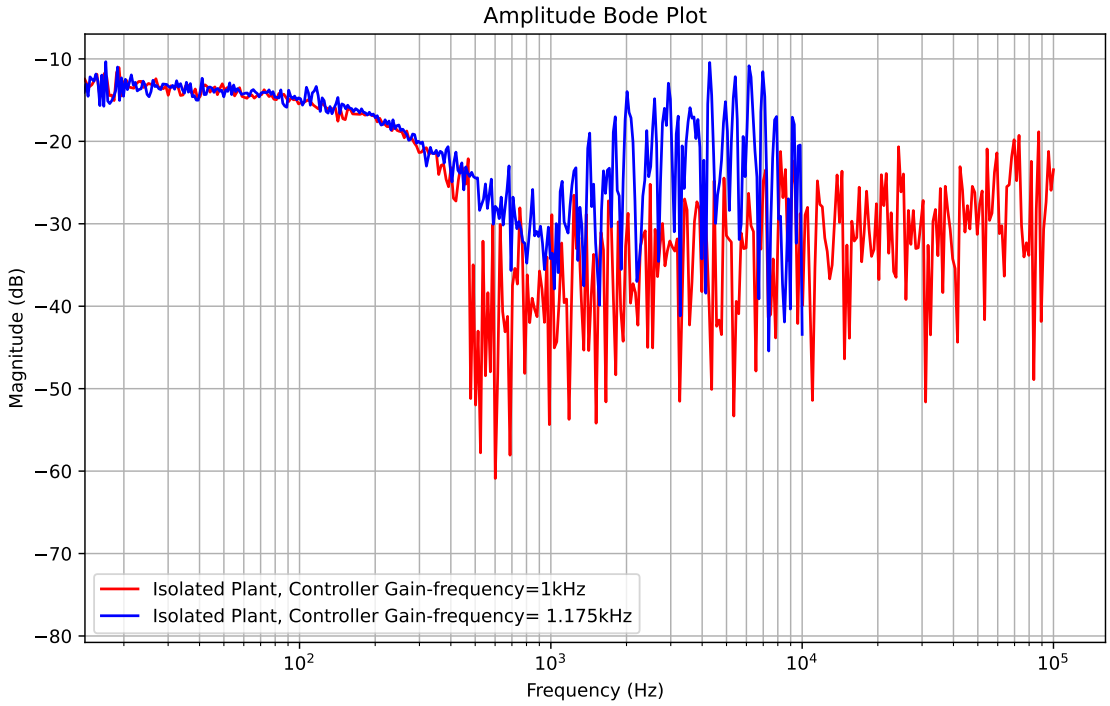

Figure 11: Amplitude Bode Plot of the PZT system

Remarks on Fig:11: The y-axis is uncalibrated. The initial dip near 10 Hz is due to temporary loss of lock and not indicative of PZT response. For this PZT, resonance is reported at 100 kHz range, and amplitude steadily decreases with frequency. Adding a mirror reduces resonant frequencies. In our case, no distinct resonance was observed between 10 Hz and 1 kHz, suggesting this frequency range is safe for driving the PZT.

However, due to stability limits in the controller(drift noise cannot be locked), we were unable to increase the gain-frequency significantly beyond 1 kHz, preventing resolution of the PZT response in higher-frequency regions.

Result

The amplitude Bode plots at 1 kHz and 1.175 kHz gain values confirm that the system responds well from 15 Hz to 1 kHz. No prominent resonant peaks were observed in this range, suggesting this bandwidth is suitable for phase modulation without significant amplitude distortion.

Future Follow-up We will proceed with squeezing measurements by driving the PZT using sinusoidal excitations at 50 Hz (within the safe range). The low-pass filter corner frequency in the lock-in amplifier can be safely set near 100 kHz for quadrature demodulation.

4.7 Technical Noise Contributions: Moku-Pro and Photodiode Noise

To reliably observe squeezing, the total system noise floor must lie below the shot noise level. If electronic noise from the acquisition system (e.g., Moku-Pro) or dark noise from the photodetectors (PDs) is comparable to or exceeds the shot noise, squeezing signatures will be obscured. Therefore, accurate noise characterization of both detection electronics and PDs is essential. Additionally, the unsqueezed shot noise level must be calibrated and, if necessary, increased by adjusting the LO power to ensure it dominates over technical noise.

4.7.1 Moku-Pro ADC Input Noise Characterization

Experiment To measure the intrinsic input noise of the Moku-Pro, Input 1 was properly terminated using a 50 Ω Micro-Circuits BRTM-50+ connector. The Spectrum Analyzer module was configured with the following settings:

- Y-axis: Vpp, PSD units
- Input range: 400 mVpp (lowest range to reduce quantization noise)
- Input impedance: 50 Ω (matched to termination)
- Coupling: DC (0–1 kHz), AC (1 kHz–300 MHz)

To improve the signal-to-noise ratio in the low-frequency regime, frame averaging was applied. The resolution bandwidth (RBD) was manually tuned across frequency segments to clearly resolve spectral features. These segmented traces were then stitched together to produce a continuous Amplitude Spectral Density (ASD) plot.

4.7.2 Photodiode Dark Noise ASD Characterization

Experiment

The room was darkened to suppress ambient light. The AC outputs of the North and South PDs were connected to Inputs 1 and 2 of the Moku-Pro, respectively, via BNC cables. The Spectrum Analyzer settings were kept identical to those used for the Moku-Pro noise measurement. Although the PDs have a 33 Ω output impedance, a 50 Ω input setting was used on the Moku-Pro to ensure impedance matching. RBD and frame averaging were again tuned for optimal spectral resolution.

Table 1: Acquisition settings for Moku-Pro and Photodetectors

Device	Frequency Range	RBW	Averaging, Coupling
Moku-Pro In-1	0–100 Hz	1.24 Hz	15 avg, DC
	100 Hz–1 kHz	5 Hz	15 avg, DC
	1–5 kHz	19.55 Hz	31 avg, AC
	5–10 kHz	24.44 Hz	55 avg, AC
	10–100 kHz	439.9 Hz	5 avg, AC
	100 kHz–3 MHz	4.5 kHz	AC
	3–10 MHz	20.31 kHz	AC
	10–50 MHz	162.5 kHz	AC
	50–300 MHz	325 kHz	AC
North/South PDs	0–500 Hz	1.24 Hz	15 avg, DC
	500 Hz–1 kHz	8 Hz	DC
	1–10 kHz	19.34 Hz	40 avg, AC
	10–50 kHz	84.63 Hz	40 avg, AC
	50–100 kHz	104.2 Hz	23 avg, AC
	100–500 kHz	846.3 Hz	23 avg, AC
	500 kHz–1 MHz	1.128 kHz	AC
	1–300 MHz	40.62 kHz	AC

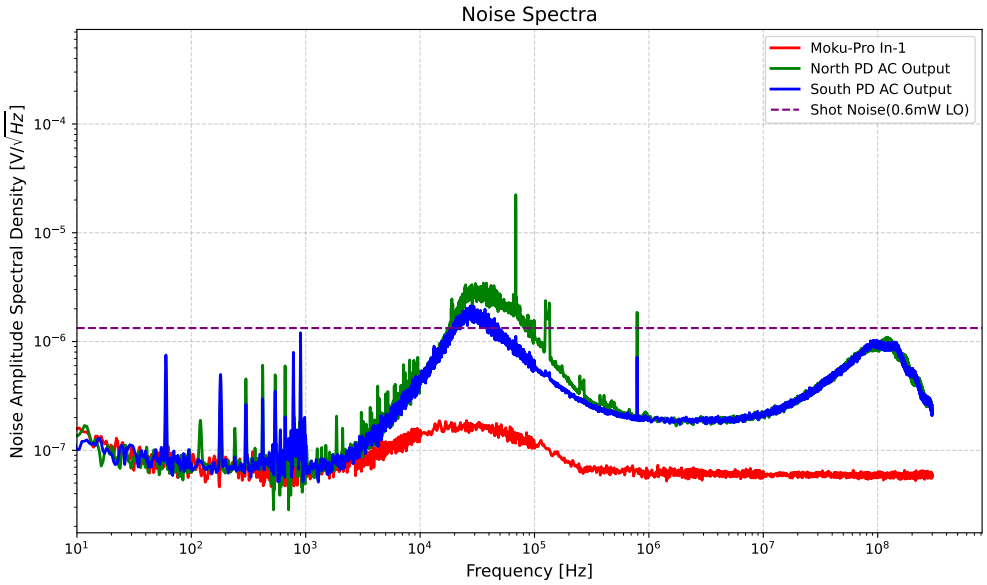

Figure 12: Amplitude spectral density (ASD) of the Moku-Pro (Input 1) and Photodetectors (North/South PDs).

Results

- The Moku-Pro input noise floor was measured to be approximately $1 \times 10^{-7}\,\mathrm{V}/\sqrt{\mathrm{Hz}}$, in good agreement with manufacturer specifications.
- A spectral peak was observed in the Moku-Pro noise between 10–100 kHz.
- The PD dark noise spectra showed prominent peaks around 80 kHz and 100 MHz, with amplitudes near $1 \times 10^{-6}\,\mathrm{V}/\sqrt{\mathrm{Hz}}$.

Future Follow-Up

With a local oscillator power of approximately 1 mW, the shot noise level will exceed both Moku-Pro and PD dark noise levels across all relevant frequency bands. Therefore, this LO power can be safely used in squeezing measurements to ensure that quantum noise dominates over technical noise.

4.8 Non-Linear Gain Measurements

Previously, Second Harmonic Generation (SHG) efficiency was used to verify phase matching and alignment of the pump with the input fiber and the waveguide axis. However, for more rigorous optimization of the waveguide orientation for squeezing experiments—we performed measurements of the non-linear gain in the seed power in an Optical Parametric Amplification (OPA) process i.e. when both seed (1064 nm) AND PUMP (532 nm) are present . Linking the non-linear gain in the seed power of OPA to the squeezing parameter would also allow us to get an estimate of the squeezing we should expect in Spontaneous parametric down conversion process.

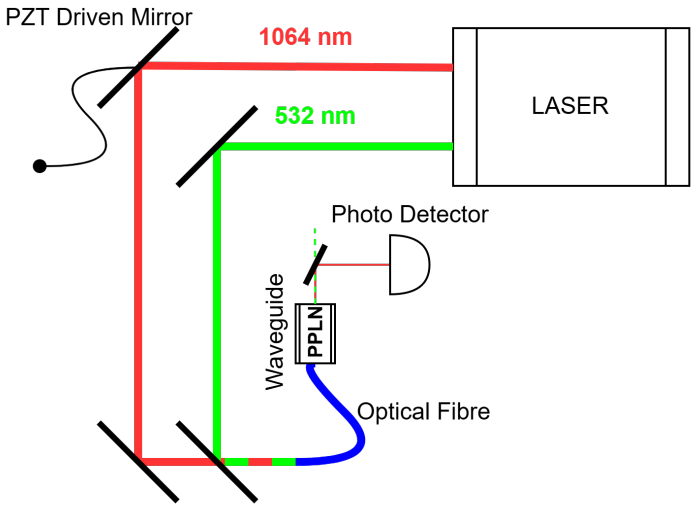

Figure 13: OPA Non- Linear Gain measurement setup

4.8.1 Experimental Method

A low-power 1064 nm signal (∼100 µW, measured at the South photodetector) and a high-power 532 nm pump (up to 5 mW) were coupled into the PPLN waveguide. The experiment proceeded as follows:

1. **Initial alignment:** Alignment was first optimized for maximum second-harmonic generation (SHG) by injecting only the 1064 nm signal and adjusting the brass fiber coupler, aspheric lens, and 1064 nm optics until SHG from the crystal was maximized.

2. **Pump alignment:** With the signal blocked, the 532 nm pump path was aligned to maximize coupled pump power. The maximum 532 nm power measured immediately after the crystal was 4.22 ± 0.2 mW.

3. **Signal conditioning:** The 1064 nm signal was attenuated with a half-wave plate to yield ∼100 µW at the South photodetector (corresponding to an ∼80 mV DC voltage on the Moku:Pro oscilloscope).

4. **Phase modulation:** To overcome slow phase drifts between pump and signal and to periodically sweep through the OPA phase-matching condition, the first spherical mirror in the signal path was mounted on a PI P180.10 PZT. The PZT was driven with a 30 Hz, 1 V_{pp} triangular waveform (500 mV DC offset) from a Siglent function generator and amplified by a high-voltage driver (gain 15, 0–150 V mode), providing a 0–15 V ramp.

5. **Data acquisition:** With both beams present, the pump power was varied from 0 to 4 mW in 0.5 mW steps while recording the South PD DC trace using the Moku:Pro oscilloscope in precision mode (400 mVpp vertical range, DC coupling, 50 Ω input).

All subsequent classical and semi-classical analyses were performed on this same data set.

4.8.2 Observations

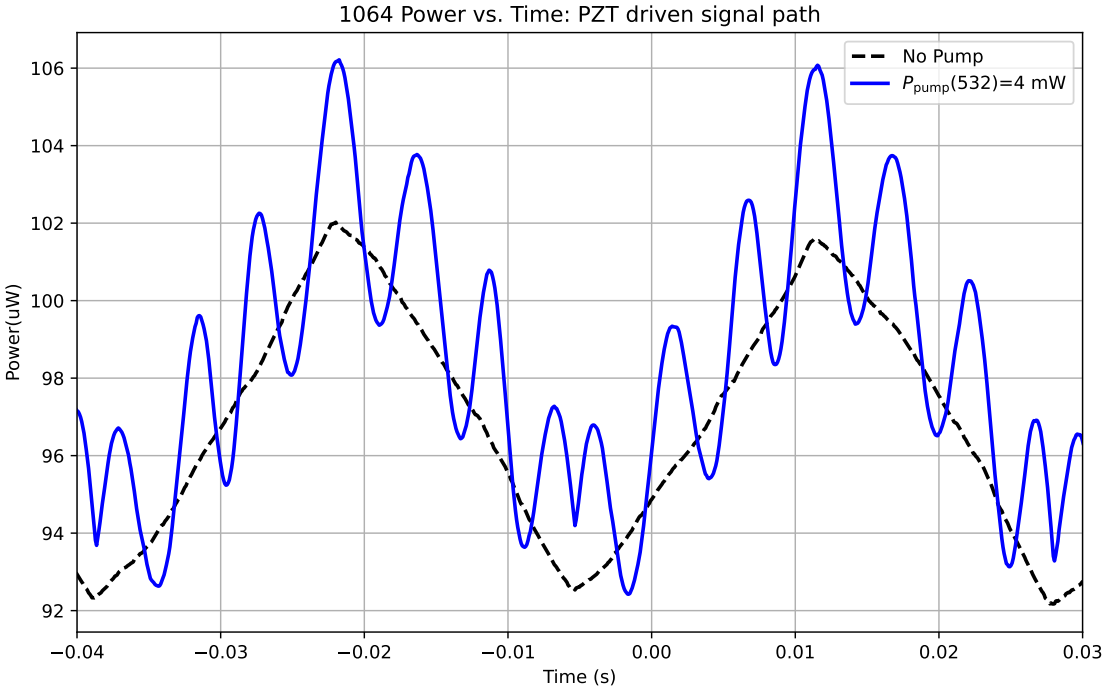

Figure 14: 1064 Power vs. Time: PZT driven signal path

- **Reference modulation:** With only the 1064 nm signal present, the PD output exhibited triangular fluctuations at the 30 Hz PZT drive frequency, arising from periodic changes in coupling efficiency due to mirror displacement.
- **OPA peaks:** When both signal and pump were incident, additional higher-frequency peaks appeared in the PD output at ∼180, 210 and 240 Hz (about 8 peaks per PZT cycle). These peaks, attributed to Optical Parametric Amplification (OPA) of the 1064 nm signal, increased in amplitude with increasing 532 nm pump power but maintained constant frequency.
- **Reference subtraction:** The 30 Hz reference modulation (measured with pump blocked) was scaled and subtracted from all data to isolate the OPA peaks from low-frequency coupling variations.

4.8.3 Nonlinear Gain Extraction

For each pump power the mean amplitude of the isolated OPA peaks was taken as the amplified 1064 nm power increment, and the variance of the peaks provided the error estimate. The experimental nonlinear gain in decibels is given by

$$\mathrm{Gain}_{\mathrm{dB}} = 10\log_{10}\left(\frac{P_{\mathrm{out}}}{P_{\mathrm{in}}}\right), \qquad P_{\mathrm{out}} = P_{\mathrm{in}} + \langle P_{\mathrm{peak}}\rangle, \tag{19}$$

where P_{in} is the 1064 nm power with pump blocked and $\langle P_{\mathrm{peak}}\rangle$ is the mean OPA peak power converted from PD voltage using the detector responsivity and oscilloscope calibration. At

a pump power of 4 mW the measured 1064 nm power gain was approximately 0.1 dB, corresponding to a ∼2–3 µW increase in output power.

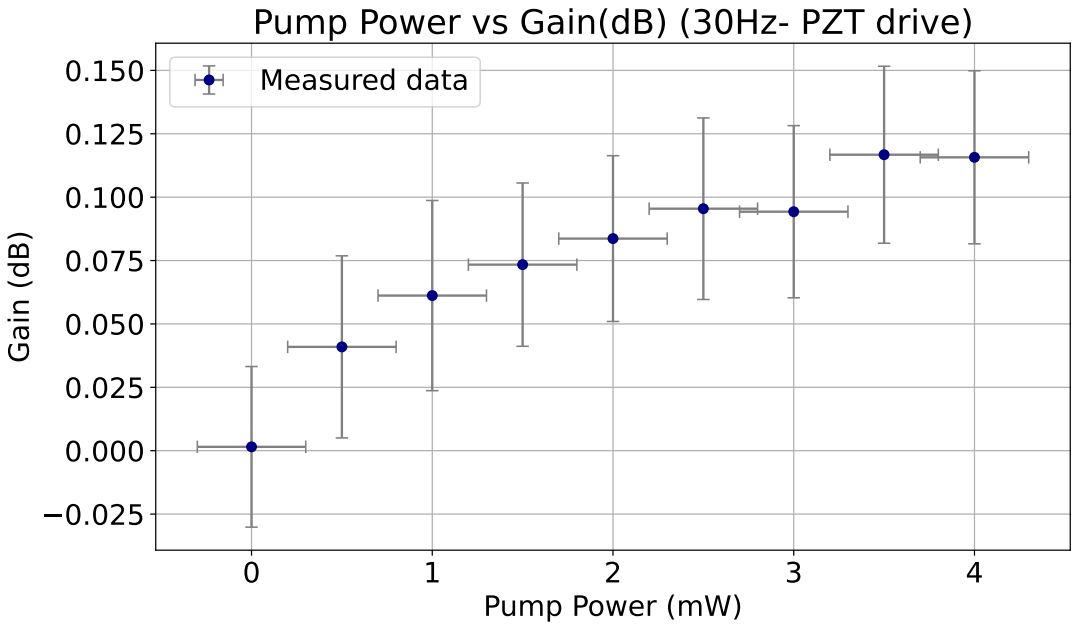

Figure 15: Non- Linear Gain in Seed Power (1064 nm) Vs Pump Power (532 nm)

4.8.4 Classical derivation of nonlinear gain in OPA

Under the undepleted-pump approximation ($E_p = \text{const.}$) and perfect phase matching ($\Delta k = 0$), the coupled-wave equations for the slowly varying complex field amplitudes $E_s(L)$ and $E_i(L)$ are:

$$\frac{dE_s}{dL} = i\, d\, \frac{\omega_s}{n_s c}\, E_p\, E_i^*, \tag{20}$$

$$\frac{dE_i}{dL} = i\, d\, \frac{\omega_i}{n_i c}\, E_p\, E_s^*. \tag{21}$$

Define the coupling constants

$$k_s \equiv d\, \frac{\omega_s}{n_s c}, \qquad k_i \equiv d\, \frac{\omega_i}{n_i c}.$$

Differentiating (20) and substituting (21) yields a second-order equation for E_s:

$$\frac{d^2 E_s}{dL^2} = k_s k_i |E_p|^2\, E_s. \tag{22}$$

Define the gain coefficient g by

$$g^2 \equiv k_s k_i |E_p|^2. \tag{23}$$

The general solution is

$$E_s(L) = A \sinh(gL) + B \cosh(gL). \tag{24}$$

For the usual boundary conditions (input idler absent $E_i(0) = 0$ and incident seed $E_s(0) = E_{s0}$) one obtains

$$E_s(L) = E_{s0} \cosh(gL), \tag{25}$$

$$E_i^*(L) = \frac{g}{ik_s E_p} E_{s0}^* \sinh(gL). \tag{26}$$

The output intensities follow as

$$I_s(L) = |E_s(L)|^2 = |E_{s0}|^2 \cosh^2(gL), \tag{27}$$

$$I_i(L) = |E_i(L)|^2 = k_s k_i |E_{s0}|^2 \sinh^2(gL). \tag{28}$$

For degenerate OPA ($\omega_s = \omega_i$) the total (signal+idler) gain relative to input signal intensity $I_{s0} = |E_{s0}|^2$ is

$$G \equiv \frac{I_s(L) + I_i(L)}{I_{s0}} = \cosh^2(gL) + k_s k_i \sinh^2(gL) = (k_s k_i + 1) \sinh^2(gL) + 1. \tag{29}$$

Here,

- E_s, E_i, E_p : Electric field amplitudes of the signal (1064 nm), idler (1064 nm), and pump (532 nm) waves.
- ω_s, ω_i : Angular frequencies of the signal and idler fields.
- n_s, n_i : Refractive indices of the waveguide for the signal and idler wavelengths.
- c : Speed of light in vacuum.
- d : Effective second-order nonlinear coefficient of the PPLN crystal, $d = \frac{2}{\pi} d_{33}$ for Type-0 quasi-phase matching.
- k_s, k_i : Effective nonlinear coupling constants for the signal and idler.
- L : Propagation distance along the PPLN waveguide (replacing z).
- g : Nonlinear gain coefficient of the OPA process.
- $|E_p|^2$: Pump intensity inside the waveguide.
- P_{pump} : Pump power at 532 nm coupled into the waveguide.
- A : Effective mode area of the pump in the waveguide.
- E_{s0} : Input signal amplitude at the crystal entrance ($L = 0$).
- P_{in} : Input signal power with the pump blocked.
- P_{out} : Amplified signal power at the output of the waveguide.
- G : Parametric gain, defined as the ratio $P_{\text{out}}/P_{\text{in}}$.

Parameter substitutions

The following parameters (taken from the manufacturer datasheet[7]) were used to produce theoretical gain estimates:

- $d = \frac{2}{\pi} d_{33}$, with $d_{33} = 25.3$ pm/V.
- $\lambda = 1064$ nm, $\omega_s = 2\pi c/\lambda$.
- $n_s \approx 2.156$ (extraordinary index; Type-0 phasematching assumed).
- Interaction length $L = 15$ mm.
- Pump field amplitude: $|E_p|^2 = P_{\text{pump}}/A$, with pump power P_{pump} and mode area $A = \pi(2.41\ \mu\text{m})(2.08\ \mu\text{m})$.

Using (23) and the above values produces a theoretical curve $G(P_{\text{pump}})$ which is compared to the experiment.

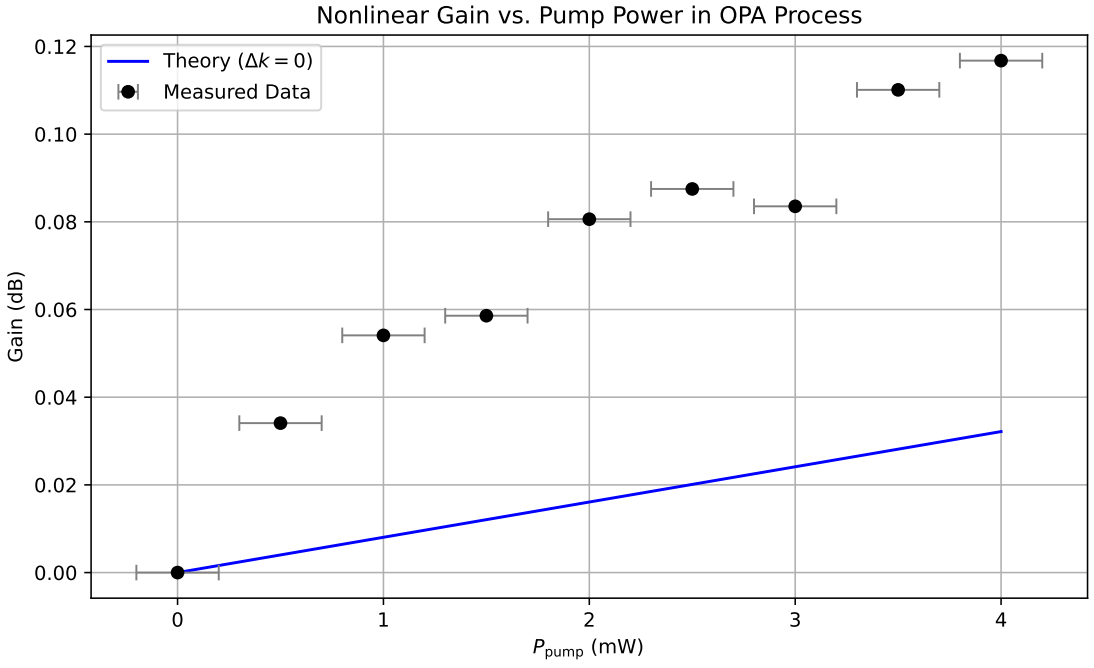

Figure 16: Non- Linear Gain in OPA with theoretical fit

The theoretical gain from (**??**) under ideal assumptions (perfect phase matching, undepleted pump, uniform poling) is slightly lower (up to ∼0.1 dB difference). Likely causes of the discrepancy include pump–seed phase drifts, and local variations in poling / phase-matching that are not included in the simple model.

4.8.5 Semi-classical derivation: extracting the squeezing parameter from measured gain

To connect classical gain to squeezing we adopt a semi-classical quadrature transformation. Denote the phase angle between pump and seed by ψ. The rotation and squeezing matrices acting on the quadrature vector are

$$R(\psi) = \begin{bmatrix} \cos\psi & \sin\psi \\ -\sin\psi & \cos\psi \end{bmatrix}, \qquad S(z) = \begin{bmatrix} e^{-z} & 0 \\ 0 & e^{z} \end{bmatrix}, \tag{30}$$

and the net transformation is

$$B = R(\psi)\, S(z)\, R^{T}(\psi) = \begin{bmatrix} e^{-z}\cos^2\psi + e^{z}\sin^2\psi & (e^{z} - e^{-z})\cos\psi\sin\psi \\ (e^{z} - e^{-z})\cos\psi\sin\psi & e^{z}\cos^2\psi + e^{-z}\sin^2\psi \end{bmatrix}. \tag{31}$$

For an input coherent seed along the x-quadrature, $\vec{\alpha} = [\alpha, 0]^T$, the output quadrature vector is

$$\vec{E}_{\text{out}} = B\vec{\alpha} = \alpha \begin{bmatrix} \sin(2\psi)\sinh z \\ \cosh z + \cos(2\psi)\sinh z \end{bmatrix}. \tag{32}$$

The output intensity (power) is proportional to the squared norm:

$$\begin{aligned} N_b = \vec{E}_{\text{out}}^{T}\vec{E}_{\text{out}} &= \alpha^2\Big[(\sin(2\psi)\sinh z)^2 + (\cosh z + \cos(2\psi)\sinh z)^2\Big] \\ &= \alpha^2\big[\cosh(2z) + \cos(2\psi)\sinh(2z)\big]. \end{aligned} \tag{33}$$

This expression exhibits the characteristic phase-sensitive amplification/deamplification of OPA.

Parameter extraction procedure

1. For each pump power the reference-subtracted PD trace was time-aligned and the OPA peaks isolated.
2. For each selected OPA peak the function (33) (with free parameters z, ψ, and an amplitude prefactor α^2) was fitted to the peak shape; the fit returns the squeezing parameter z and phase ψ.
3. The fitted z is converted to squeezing in decibels by

$$\text{Squeezing (dB)} = -10\log_{10}\left(e^{2z}\right) = -\frac{20}{\ln 10}\, z. \tag{34}$$

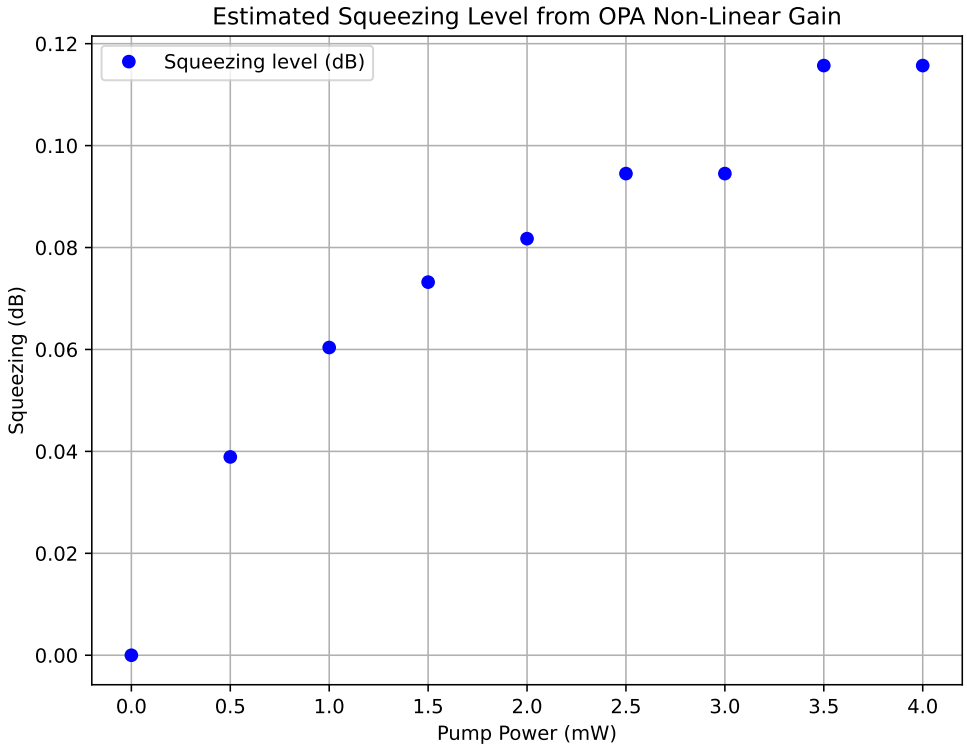

Figure 17: Estimated Squeezing Level from OPA Non-Linear Gain

4.8.6 Results and Conclusions

- The OPA experiment yielded a measured 1064 nm power gain of approximately 0.1 dB at a pump power of $P_{\text{pump}} = 4$ mW.
- The classical coupled–wave model predicts a similarly small gain in this low-power regime. The observed excess output (2–3 μW above theory) is likely due to residual phase mismatch between the 1064 nm seed and the 532 nm pump that was not fully captured in the model.
- A semi-classical fit to the OPA gain peaks provides a squeezing parameter consistent with the measured value, giving an estimated squeezing of ~ 0.1 dB at $P_{\text{pump}} = 4$ mW. This indicates that the low squeezing level arises primarily from limited squeezed-light generation (e.g., poor waveguide coupling or imperfect mode matching) rather than from detection errors in the balanced-homodyne setup.
- The measured WOPA gain serves as a practical *in-situ* metric for optimizing alignment and polarization during squeezing experiments. By maximizing the OPA non-linear gain (up to $\sim 14\%$), all optics before the crystal were carefully aligned and the input polarizations of the 1064 nm signal and 532 nm pump were tuned for optimal coupling, which is expected to improve subsequent squeezing performance.

5 Future Goals & Conclusion

Future Goals

- **Fiber-Induced Polarization Drift Diagnosis:** $\sim 80\%$ loss in 532 nm power was observed when passing through the fiber and waveguide. Replace the existing fiber with a single-mode fiber and compare the transmission performance to diagnose polarization drift. Try free space coupling with the waveguide.
- **Mode Matching:** Use Gaussian beam propagation tools (e.g., `Finesse` or the ABCD matrix formalism) to model the 1064 nm signal and local oscillator (LO) paths. Experimentally align the system to achieve $> 95\%$ spatial overlap at the beam splitter in the balanced homodyne detector (BHD), and verify the overlap using beam profiling measurements.
- **Fast Squeezing Measurement:** Increase the pump power and implement fast squeezing detection using lock-in amplification. Filter the sideband frequency to below 100 kHz and modulate the LO path with a PZT-driven mirror actuated by a 50 Hz sine-wave signal.

Conclusion

This work investigated the generation of squeezed vacuum states using a **Waveguided Optical Parametric Amplifier (WOPA)** based on a PPLN waveguide pumped at 532 nm. Over the summer, we performed a complete experimental characterization, including **balanced homodyne detection of squeezing**, measurement of **nonlinear OPA gain**, and development of a preliminary **noise budget**.

Coupling inefficiencies, polarization drift, and mode mismatch were identified as the primary factors limiting the observed squeezing. Balanced homodyne detection revealed a squeezing level of approximately **0.1 dB** at a 4 mW pump power. Nonlinear gain measurements of the optical parametric amplifier showed a 1064 nm power gain of **0.1 dB**, consistent with classical coupled-wave predictions and validating the gain model. A semi-classical analysis of the OPA peaks yielded a squeezing parameter in close agreement with direct measurements, indicating that the limited squeezing originates from weak nonlinear interaction and coupling inefficiencies rather than detection errors. Maximizing the OPA gain proved to be an effective in-situ metric for alignment and polarization optimization, providing a practical pathway to improve future squeezing levels.

These results establish a clear experimental baseline for WOPA-based squeezing and outline key steps—such as increasing pump power, enhancing mode matching, and stabilizing polarization—required to achieve stronger squeezing. The methods developed here contribute toward the broader goal of realizing compact, cavity-free squeezed-light sources for broadband quantum-noise reduction in gravitational-wave observatories such as LIGO.

References

[1] K. P. Zetie, S. F. Adams, and R. M. Tocknell, *How does a Mach–Zehnder interferometer work?*, Physics Education **35**(1), 46–48 (2000).

[2] K. McKenzie, *Squeezing in the Audio Gravitational Wave Detection Band*, Ph.D. thesis, The Australian National University (2008).

[3] K. Goda, *Development of Techniques for Quantum-Enhanced Laser-Interferometric Gravitational-Wave Detectors*, Ph.D. thesis, Massachusetts Institute of Technology (2007).

[4] M. C. Teich and B. E. A. Saleh, *Squeezed States of Light*, Quantum Optics: Journal of the European Physical Society B **1**, 153–191 (1989); reprinted in *Tutorials in Optics*, ed. D. T. Moore (Optical Society of America, 1992), ch. 3, pp. 29–52.

[5] M. Tse *et al.*, *Quantum-enhanced advanced LIGO detectors in the era of gravitational-wave astronomy*, Phys. Rev. D **104**, 062006 (2021).

[6] LIGO Laboratory, *LIGO Caltech Website*, https://www.ligo.caltech.edu/

[7] HC Photonics Corp. PPLN Waveguide Manual

[8] LIGO Scientific Collaboration, *Advanced LIGO Noise Budget Documentation*, LIGO Technical Resource, https://noisebudget.docs.ligo.org/aligoNB/, accessed June 2025.

[9] R. W. Boyd, *Nonlinear Optics*, 3rd Edition, Academic Press, Burlington, MA (2008).